Experimental characterization of a canonical two-fluid coaxial atomizer

P. D. Huck*,N. Machicoane, R. Osuna-Orozco, A. Aliseda
Department of Mechanical Engineering, University of Washington, USA

Abstract

We investigate the break-up and spray development of a liquid jet by a high-speed turbulent coaxial gas jet under a wide range of gas Reynolds numbers and swirl ratios. Despite its extended use in engineering and natural processes to generate a high quality spray, the instabilities that control the liquid droplet size and their spatio-temporal distribution in coaxial atomization are not fully understood. This quantitative understanding is necessary for a first-principles approach to spray control. We present measurements of the liquid interface instability (wavelength and break-up frequency) and droplet size and velocity distributions in the near- and mid-field of a canonical coaxial gas-liquid atomizer. The liquid jet is kept laminar, while the gas-to-liquid momentum ratio varies from 5 to 375 and the gas-phase Reynolds is between 21,200 and 180,000. The gas boundary layer velocity at the exit of the nozzle is measured using a combination of hot-wire anemometry in the absence of liquid, resolving the boundary layer thickness and the azimuthal to axial momentum ratio that causes the three-dimensionality of the flow in the swirl cases. The development of the hydrodynamic instabilities on the liquid-gas interface is quantified using high speed visualizations at the exit of the nozzle and related to the frequency and growth rates predicted by stability analysis of this boundary layer flow. The resulting spray structure is characterized and compared to stability analysis statistical predictions, and will be compared to Large Eddy Simulations simulations of the mid-field by our ONR-MURI collaborators at University of Florida.

Introduction

Liquid sprays are a fundamental tool in the study of engineering processes involved in food processing, coating, printing, and fire safety. Arguably, one of the most common applications in engineering practice is combustion and, to date, the control of fuel sprays from formation to mid-field dispersion, especially in the context of multiphysics actuation is still an open question. In this contribution, we investigate a co-axial two-fluid canonical atomizer which is capable of creating any desired distribution of dispersed liquid phase in the mid-field. This canonical situation is also investigated using radiographic measurements [1, 2, 3] and computational simulation [4]. We investigate the mean and fluctuating gas-phase velocities as well as maps related to the probability of liquid phase presence in the near field and characterize standard measures of spray topology such as the opening angle and virtual origin. Interestingly, these metrics present Reynolds number dependencies that are different than a pure gas-phase jet.

Experimental Methods

We present a canonical atomizer fed by eight gas inlets, four of which are off axis and can create a swirling jet with a tunable swirl ratio. The central needle for liquid injection allows coaxial gas-liquid atomization (fig. 1, a). The diameter of the the air jet is $D_g = 10$ mm while the outer diameter of the liquid jet is $D_l = 3$ mm with a gap of $h = 3.5$ mm. Reynolds numbers based on the liquid phase characteristics are in the range $Re_l = v_l D_l / \nu_l = [700 - 3700]$, while those based on the gas phase conditions span $Re_g = v_g D_g / \nu_g = [21200 - 180000]$, where v_l (v_g), D_l (D_g), and ν_l (ν_g) are the liquid (gas) nozzle velocity, diameter, and kinematic viscosity. The atomizer may be tuned to obtain variable momentum flux ratios: $M = (\rho_g v_g^2)/(\rho_l v_l^2) = [5 - 375]$ with volume fractions of $\phi_v = Q_{vl}/(Q_{vg} + Q_{vl}) = [.1 - 10] \times 10^{-4}$ where $Q_{vl} = v_l S_l$ and $Q_{vg} = v_g S_g$ are the liquid and gas volume fluxes where S_l and S_g are the respective surface areas through which each phase is injected.

In order to study the topological evolution of the gas phase with downstream distance and the degree to which self-similarity is obtained in our canonical atomizer, we employ standard Hot-Wire Anemometry (HWA) techniques. With the elevated volume fractions used here, the liquid and gas phases are likely to be strongly coupled and high speed films are taken with a Phantom V.12 (Vision Research, 1Mpixel@6800 frames per second) camera to obtain a series of instantaneous images in the near-field (up to $3D_g$) of the spray. The spray is back-lit by a 25 W LED focused white light source in the optical axis of the high-speed camera, resulting in shadowgraph images (such as the one shown in fig. 3,a) permitting a distinction between the liquid and gas phase appearing as dark and light regions, respectively. In what follows, we compare results of the gas and liquid phases to present

---

*Corresponding author: huckp@uw.edu

an overall picture of the spray structured produced by this canonical atomizer under a wide range of operating condition.

(a)

(b)
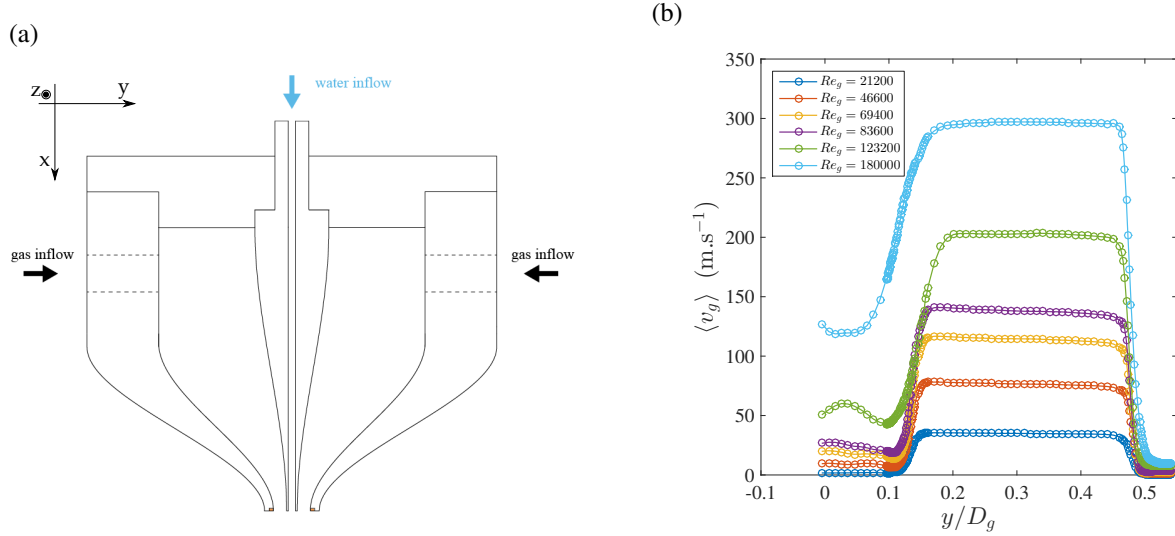
Figure 1. The Canonical Atomizer. (a) CAD drawing of the Canonical Atomizer. (b) Boundary layer measurements collected using Hot-Wire Anemometry 0.25 mm downstream of the nozzle exit, over a wide range of Reynolds numbers.

Results and Discussion

HWA is used to measure the streamwise velocity component in the single phase gas annular jet. The raw velocity profile measured is plotted along a radial component, y, passing through the boundary of the liquid needle and through the gas annulus into the outer entrainment region in figure 1,b) for the range of Re_g studied here. The boundary layer thickness, δ, measures the extend of the momentum deficit caused by the no-slip condition, and propagated by viscosity. This metric is known to be well represented by a power law of the Reynolds number, $\delta/h \propto Re^{-1/2}$, in a turbulent flow[5], and is the dominant variable in the Kelvin-Helmholtz instability that initiates the cascade of events that lead to atomization in this injectors, controlling the characteristic droplet sizes in the

(a)

(b)
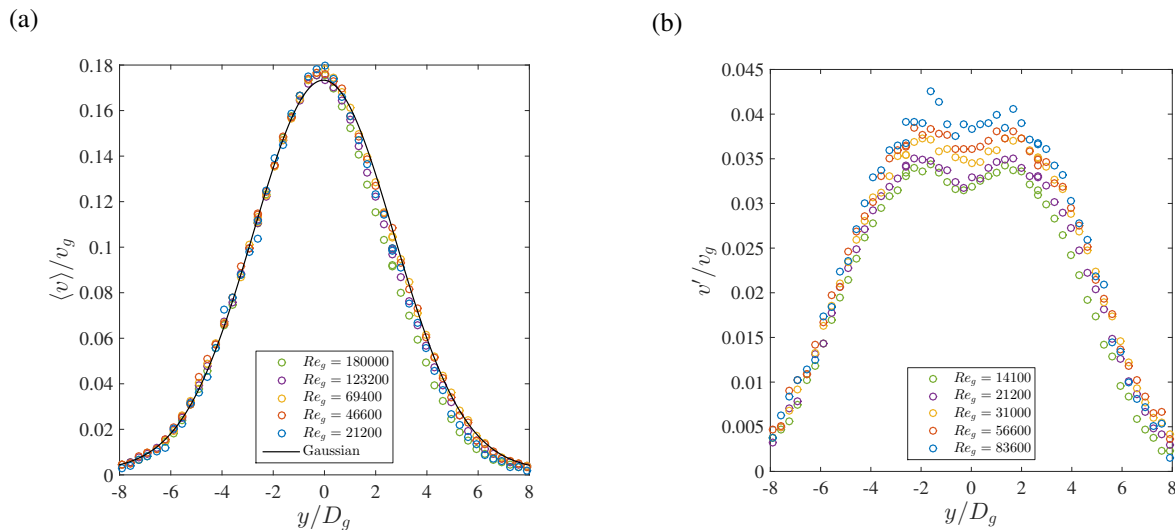
Figure 2. Far-field ($x/D_g = 30$) gas phase velocity profiles where the velocity has been decomposed into a mean and fluctuating part: $v_g = \langle v_g \rangle + v_g'$. $M = [5, 25, 80, 174, 370]$. (a) Mean field velocity ($\langle v_g \rangle$) profiles are self-similar in the far-field and well approximated by a Gaussian curve. (b) Fluctuating (v_g') velocity are nearly self-similar in the far-field, though the collapse is only partial for the lowest Reynolds numbers.

(a)   (b)
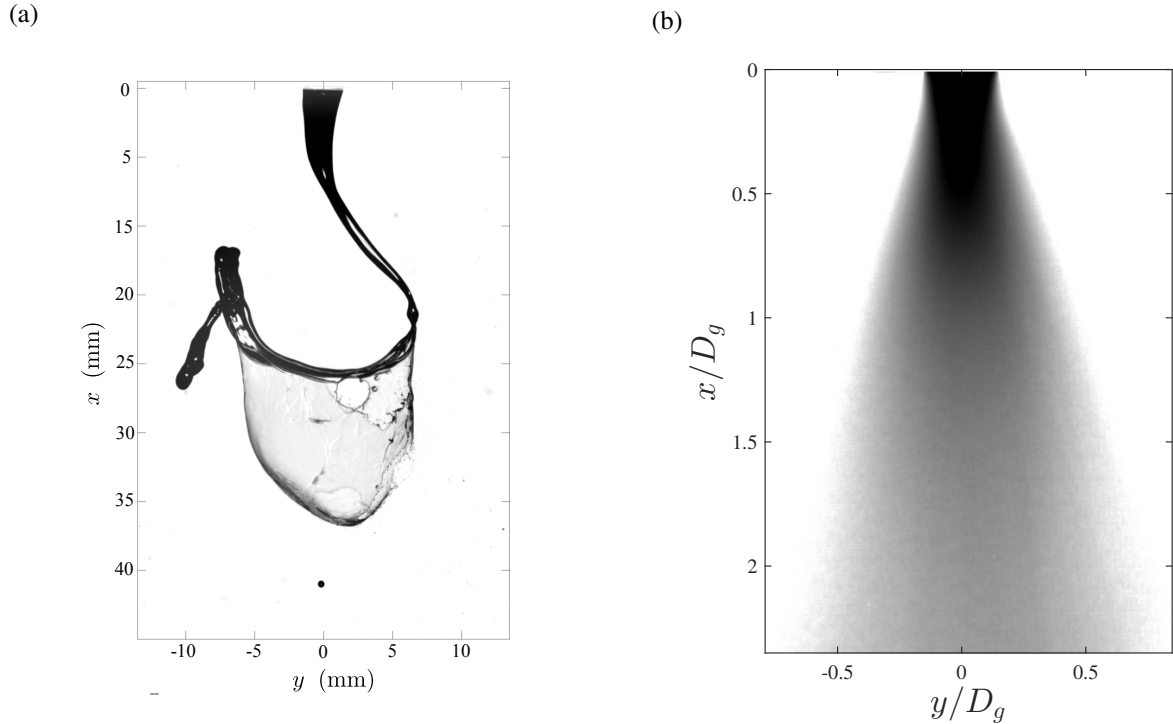
Figure 3. Shadowgraph images. (a) High speed image using the Shadowgraph technique of at $Re_g = 10600$ and $M = 1.1$. (b) Average pixel intensity $\langle I \rangle$ of images from the $Re_g = 31000$ and $M = 11$. The average pixel intensity is related to the probability that the liquid phase is present at a given point in the image with the white background indicating low probability and dark regions indicating a high probability of the finding the liquid phase present.

far-field produced by this type of high Weber number liquid break-up dominated by the gas momentum (high M and low m[6]). The boundary layer profiles shown in figure 1(b) share similar qualitative characteristics, typical of a turbulent channel flow in the gas annular nozzle. Quantitatively, the radial profiles collapse collapse well upon normalization by the typical nozzle velocity, v_g, and the boundary layer thickness estimated from the measurements and the canonical scaling indicated above. When the velocity measurements are decomposed into a mean velocity, v_g, and a fluctuating part, $v_g = \langle v_g \rangle + v'_g$, similar collapse is observed in the mean velocity profile (fig. 2 a) and the root mean square of the fluctuating (fig. 2 b) at $x/D_g = 30$, with collapse in mean quantities occurring close to the nozzle and further down for higher order statistics. In all cases the collapsed profiles are fit well by a Gaussian function.

The collapse of the gas fluctuating velocity component rms, v'_g, is not appreciable until the farthest downstream positions measured ($x/D_g = 30$, fig. 2, b), and even then it is not fully converged. Interestingly, this radial profile of velocity fluctuations (fig. 2, b) differs from the typical Gaussian profile, presenting two local maxima, a similar topology to the boundary layer formed at the splitting plate of the atomizer(see figure 1,b), in agreement with the measurements in canonical turbulent wakes [8]. Evidently, the collapse in v'_g is partial and the fluctuating velocity profiles do not seem to have completely lost the signature from the initial annular gas nozzle boundary layer profile. Full self-similarity in the velocity fluctuations is only expected farther downstream, as the initial conditions arising from the annular gas nozzle boundary layer are no longer are apparent in the radial profiles.

Our Shadowgraph images focus on the near field of the spray ($x/D_g = [0 - 2.5]$), where the mean velocity field was shown to be self-similar and well described by a Gaussian radial profile. An typical image taken at $Re_g = 10,600$ is shown in figure 3(a). It displays bag-breakup, a typical break-up topology that dominates at low gas Reynolds numbers/ gas-to-liquid momentum ratios. The typical regime investigated in this contribution, however, is the Kelvin-Helmholtz/Raleigh-Taylor instability break-up that dominates atomization at higher Reynolds numbers[6]. The strong contrast between the background (white) and regions where the liquid is present (black) allows for the calculation of the average light intensity in the atomizer near-field. The average light intensity $\langle I \rangle$ is a proxy for the probability that the liquid phase is present at any focal depth along a given optical path to the camera/lens. A map of this metric is plotted in figure 3(b), where the darkest regions represent elevated liquid phase

probability with respect to the white regions. Note that the light intensity maps are presented in logarithmic scale. Interestingly, radial intensity profiles are found to be Gaussian as early as $x/D_g = 0.4$, as shown by the red solid lines that satisfactorily fit the experimental points plotted in figure 4(a). These profiles present the average light intensity normalized by the maximum value on a radial profile, $\langle I \rangle / I_o$, and range between 0 and 1 at the maximum value (each plot has been shifted by 0.2 for clarity). Each pair of big red circles on the radial profiles denotes the two standard deviation width. It is clear that, as one moves farther downstream, the radial profiles broaden, which is quantified by the commensurately large values of the standard deviation. If we restrict the analysis to the velocity profile at $x/D_g = 2.3$, and plot the normalized light intensity radial profiles for different Reynolds numbers, we observe that they are all self-similar (fig. 4,c) and fit well by a Gaussian function. Reynolds number self-similarity is not unique to the data at this position; collapse occurs as soon as the intensity radial profile becomes Gaussian, typically at or slightly downstream of $x/D_g = 0.4$. These observations indicate that the dispersive capacity of the annular jet, or its ability to fill a volume of space with liquid droplets can be described by the standard deviation of the Gaussian profile used to fit the light intensity (representing the probability of liquid presence), which increases linearly with the distance downstream from the atomizer.

To illustrate this observation, the opening angle θ of the intensity profiles (fig. 3,b) is investigated at varying Reynolds numbers. To define this quantity, we mark the two-standard-deviation points in the Gaussian profiles of light intensity, for different distances downstream from the atomizer, as shown by the red circles in figure 4(b). We can then fit a linear function to those points. The point at which these two linear fits (one on each side of the light intensity Gaussian profile) cross is defined as the spray virtual origin. This process allows for the calculation of the spray spreading angle θ and virtual origin x_{vo} as a function of the Reynolds number, as pictured in figure 4(d) and inset. The spray spreading angle is a decreasing function of gas Reynolds number, consistent with observations in the literature [7]. The evolution of the spreading angle from $25°$ at the lowest Reynolds to less than $5°$ at the highest Re_g is in contrast with the universally accepted value of $11°$ in a pure gas phase jet [8]. This decrease in the spray spreading angle coincides with a progressive reduction in the value of the virtual origin (x_{vo}), which can be interpreted as moving inside the nozzle beyond a critical Reynolds number (see figure 4,d inset). The virtual origin dependency on gas Reynolds number is reminiscent of the evolution of this parameter, moving inside the nozzle, for the single phase turbulent jet. The contrast between the topological characterization of single phase jet and the measurements in this coaxial gas-liquid atomizer underline the complex nature of this multiphase flow.

Summary and Conclusions

In this contribution, we have studied the topological organization of a canonical two-fluid co-axial atomizer. The boundary layer was first investigated and good agreement with classical scaling laws was observed. The radial profiles of the mean longitudinal velocity profiles were seen to be self-similar and fitted well by a Gaussian curve in both the near and far field regions. Collapse of the fluctuating velocity profiles, however, is approximate, and then only in the far field, where the initial conditions imposed by the annular gas nozzle have been erased away. High speed imaging was used to create maps of the average light intensity in the near field of the atomizer. This metric is related to the probability that the liquid phase is present along a given light path into the camera optics. The normalized intensity profiles were found to be described well by Gaussian fits as early as $x/D_g = 0.4$. The standard deviation of these curves was seen to be an increasing function of distance from the atomizer and was used to define the spray spreading angle θ and virtual origin from the light intensity maps. Notably, the spreading angle is a decreasing function of Re_g, in contrast with the spreading angle of a single phase jet, which is known to be a universal constant in fully developed turbulence. This difference highlights the complexity of the multi-phase flow investigated here and merits further study using Particle Phase Doppler Anemometry where liquid phase droplet velocity and number density will be measured and compared directly to the gas-phase velocity. Comparison with Large Eddy Simulations will be particularly valuable, in comparing the statistical relationship of the gas and liquid phase, notably the spray structure measured simultaneously in both phases.

Acknowledgements

(a)

(b)

(c)

(d)
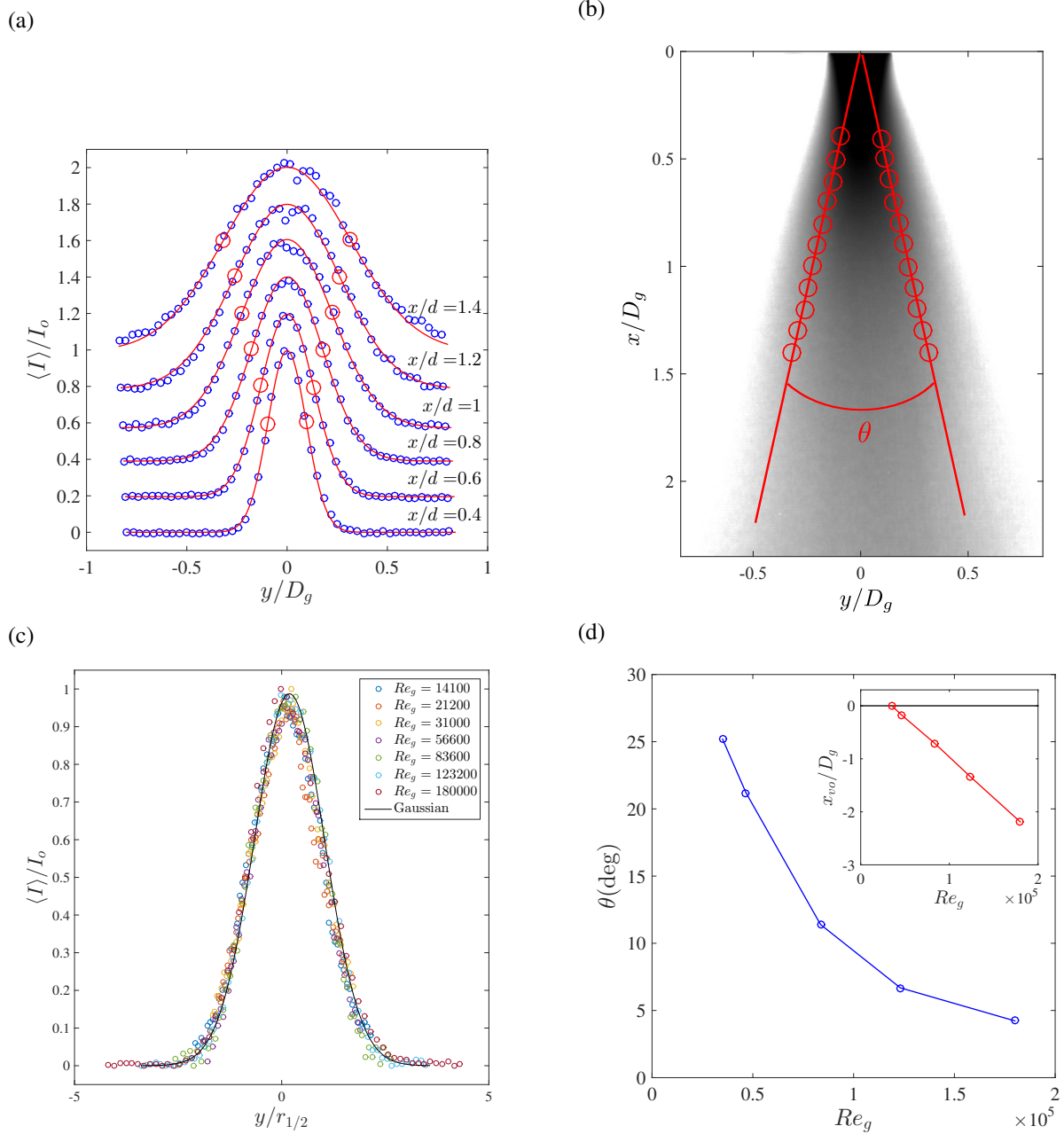
Figure 4. Topological investigation of the liquid-gas phase jet. (a) Normalized pixel intensity profiles (○) are represented with several transverse Gaussian profiles of the normalized pixel intensity $\langle I \rangle / I_o$ superimposed (red curves). Each profile passes through two circles representing a two standard deviation width. $Re_g = 31000$ and $M = 11$. (b) The increasing values of the transverse standard deviation of normalized average pixel intensity is used to define the opening angle θ by linear extrapolation. The virtual origin of the liquid-gas phase jet is defined as the point at which the two linear profiles cross. (c) Normalized pixel intensity curves at $x/D_g = 2.3$ for several different Reynolds numbers. The spatial parameter $r_{1/2}$ refers to the position at which $\langle I \rangle / I_o = 0.5$. The black line is a Gaussian fit. The corresponding momentum fluxes are: $M = [2, 5, 11, 25, 80, 174, 370]$ (d) The opening angle θ is a decreasing function of the Reynolds number. The corresponding momentum fluxes are $M = [11, 25, 80, 174, 370]$. (d,inset) As the Reynolds number increases the virtual origin moves from the near field of the jet to the interior of the atomizer. A critical Reynolds number $Re_g = 31000$ occurs where the virtual origin is at the atomizer.

References

[1] Bothell, J. K., Li, D., Morgan, T. B., Heindel, T. J., Aliseda, A., Machicoane, N., Kastengren, A., *14th Triennial International Conference on Liquid Atomization and Spray Systems*, Chicago, Illinois, July 22-26, 2018.

[2] Li, D., Bothell, J. K., Morgan, T. B., Heindel, T. J., Aliseda, A., Machicoane, N., Kastengren, A., *14th Triennial International Conference on Liquid Atomization and Spray Systems*, Chicago, Illinois, July 22-26, 2018.

[3] Morgan, T. B., Bothell, J. K., Li, D., Heindel, T. J., Aliseda, A., Machicoane, N., Kastengren, A., *14th Triennial International Conference on Liquid Atomization and Spray Systems*, Chicago, Illinois, July 22-26, 2018.

[4] Vu, L. X., Chiodi, R., Desjardins, O. *14th Triennial International Conference on Liquid Atomization and Spray Systems*, Chicago, Illinois, July 22-26, 2018.

[5] Marmottant, P., and Villermaux, E. *The Journal of Fluid Mechanics* 498: 73-111 (2018).

[6] Aliseda, A., Hopfinger, E. J., Lasheras, J. C., Kremer, D. M., Berchielli, A., and Connolly, E. K., *International Journal of Multiphase Flow*, 34:161-175 (2008).

[7] Baillot, F., Blaisot, J. B., Boisdron, G., and Dumouchel, C., *The Journal of Fluid Mechanics*, 650:305-342 (2009).

[8] Pope, S. B., *Turbulent Flows* Cambridge University Press, 2000.